

Original Research

Ibrutinib Contributes to Atrial Arrhythmia through the Autophagic Degradation of Connexins by Inhibiting the PI3K-AKT-mTOR Signaling Pathway

Huiyuan Qin^{1,†}, Bingyu Zheng^{1,†}, Zhiqiao Lin^{1,†}, Yumeng Ji², Cheng Wang¹, Huayuan Zhu³, Chang Cui^{1,*}, Zidun Wang^{1,*}, Minglong Chen¹

Academic Editor: Natascia Tiso

Submitted: 11 December 2023 Revised: 14 March 2024 Accepted: 29 March 2024 Published: 22 May 2024

Abstract

Background: Ibrutinib could increase the risk of atrial fibrillation (AF) in chronic lymphocytic leukemia (CLL) patients. However, the precise mechanism underlying ibrutinib-induced AF remains incompletely elucidated. Methods: We investigated the proportion of ibrutinib-treated CLL patients with new-onset AF. Optical mapping was conducted to reveal the proarrhythmic effect of ibrutinib on HL-1 cells. Fluorescence staining and western blot were used to compare connexins 43 and 40 expression in ibrutinib-treated and control groups. To identify autophagy phenotypes, we used western blot to detect autophagy-related proteins, transmission electron microscopy to picture autophagosomes, and transfected mCherry-GFP-LC3 virus to label autophagosomes and lysosomes. Hydroxychloroquine as an autophagy inhibitor was administered to rescue ibrutinib-induced Cx43 and Cx40 degradation. Results: About 2.67% of patients developed atrial arrhythmias after ibrutinib administration. HL-1 cells treated with ibrutinib exhibited diminished conduction velocity and a higher incidence of reentry-like arrhythmias compared to controls. Cx43 and Cx40 expression reduced along with autophagy markers increased in HL-1 cells treated with ibrutinib. Inhibiting autophagy upregulated Cx43 and Cx40. Conclusions: The off-target effect of ibrutinib on the PI3K-AKT-mTOR signaling pathway caused connexin degradation and atrial arrhythmia via promoting autophagy. Clinical Trial Registration: ChiCTR2100046062, https://clin.larvol.com/trial-detail/ChiCTR2100046062.

Keywords: ibrutinib; atrial fibrillation; connexins 43; connexins 40; autophagy

1. Introduction

Bruton's tyrosine inhibitor ibrutinib is notable efficacy against B-cell malignancies. Nonetheless, pivotal trials, roughly 5-9% of chronic lymphocytic leukemia (CLL) patients developed atrial fibrillation (AF) compared to 0.5–2.4% in controls [1]. A comprehensive investigation based on the VigiBase database (International pharmacovigilance database) included 13,572 patients who were treated with ibrutinib and aimed to characterize adverse cardiovascular effects that were associated with ibrutinib, such as supraventricular arrhythmias, ventricular arrhythmias, and conduction disorders. In total, 957 (7.07%) individuals experienced supraventricular arrhythmia, which accounted for the largest proportion of ibrutinib-associated adverse cardiovascular events [2]. Notably, AF frequently prompted the discontinuation of ibrutinib therapy. The majority of extant studies comprise observational trials wherein AF diagnosis often necessitated hospitalization or other interventions, rather than systematic long-term electrocardiogram (ECG) screening. Consequently, it is conceivable that the true incidence of ibrutinib-associated AF

may be underestimated, underscoring the imperative for further research to ascertain a more precise incidence rate [3].

The reason why ibrutinib increases the occurrence of atrial fibrillation remains inadequately elucidated. Existing studies have suggested have reported that structural remodeling via changes in gap junction protein expression could contribute to the development of AF [4]. Gap junction proteins can simultaneously mediate action potential propagation between cardiomyocytes and ensure cardiac electromechanical activity [5,6]. Within the connexin protein family, comprising 21 isoforms expressed in the human heart [7]. Among these isoforms, Cx43 stands out as the principal isoform and is widely expressed in the ventricle [8], and Cx40 is the predominant connexin protein that is mostly expressed in the atrium and conduction system. Both Cx40 and Cx43 are casually linked to a proarrhythmogenic substrate [9]. Changes in Cx40 and Cx43, including changes in their abundance, subcellular distribution and function, significantly contribute to atrial cardiomyocyte electrical remolding and thereby cause atrial arrhythmia by blocking unidirectional conduction and decreasing conduction veloc-

¹Division of Cardiology, The First Affiliated Hospital of Nanjing Medical University, 211166 Nanjing, Jiangsu, China

²Department of Cardiovascular Surgery, The First Affiliated Hospital of Nanjing Medical University, 211166 Nanjing, Jiangsu, China

³Department of Hematology, The First Affiliated Hospital of Nanjing Medical University, 211166 Nanjing, Jiangsu, China

^{*}Correspondence: cuichang@njmu.edu.cn (Chang Cui); wangzidun@njmu.edu.cn (Zidun Wang)

 $^{^{\}dagger}\textsc{These}$ authors contributed equally.

ity [10]. However, the precise impact of ibrutinib on structural alterations within cardiomyocytes, including modifications in gap junction localization and expression, remains unclear.

Autophagy, a catabolic process, involves the sequestration of cellular components within autophagosomes, facilitating the recycling of cellular constituents and preservation of cellular homeostasis [11]. Both autophagy and ubiquitination mechanisms play pivotal roles in the proteolysis of the Cx43 protein [12]. Particularly under conditions of nutrient deprivation, a classical inducer of autophagy, Cx43 can bind to the autophagy-related protein ATG5, which causes the internalization of Cx43 and further enhances its regulatory effect on autophagy [13,14]. The PI3K-AKT pathway holds paramount importance in cardiac stress responses. Notably, ibrutinib has been reported to modulate this pathway by targeting the alpha-subunit of PI3K and downregulating AKT expression [15]. Furthermore, the off-target effect emerges as a significant mechanism underlying ibrutinib-induced atrial fibrillation. Recent findings by Xiao et al. [16] have identified C-terminal Src kinase (CSK) as a crucial off-target inhibition site of ibrutinib, with CSK knockout mice exhibiting a phenotype akin to atrial fibrillation induced by ibrutinib [16]. Additionally, several studies have implicated the involvement of the PI3K-AKT-mTOR pathway in the off-target effects of ibrutinib [17,18]. Nevertheless, it remains uncertain whether the off-target impact of ibrutinib on such pathways augments autophagic activity, leading to the degradation of cell gap junction proteins Cx40 and Cx43. Thus, we conducted clinical and experimental investigations to elucidate ibrutinib-induced arrhythmogenesis and the potential role of autophagy-mediated connexin degradation in this pathophysiological process.

2. Materials and Methods

2.1 Clinical Investigation

A cohort comprising 187 patients diagnosed with CLL administered ibrutinib (single-agent, 420 mg, once daily, continuously) were enrolled in the Chronic Lymphoid Leukemia Center of the First Affiliated Hospital of Nanjing Medical University from March 2019 to March 2020. All of the patients required treatment according to the International Workshop on CLL (iwCLL) criteria [19]. Cardiovascular function was assessed by electrocardiogram and echocardiography in all patients upon admission. Throughout the 12-month follow-up period, electrocardiograms were systematically conducted every three months to monitor the incidence of arrhythmias attributed to ibrutinib.

2.2 Cell Culture

HL-1 cells obtained from Dr. William Claycomb (Louisiana State University, New Orleans, LA, USA) were validated by STR profiling and tested negative for my-

coplasma and cultured in Claycomb medium (51800C, Sigma Aldrich, St. Louis, MO, USA) supplemented with penicillin-streptomycin solution (C0222, Beyotime, Shanghai, China), 10% fetal bovine serum (F2442, Sigma Aldrich), 2 mM L-glutamine (G7513, Sigma Aldrich), and 0.1 mM norepinephrine (A0937, Sigma Aldrich) [20]. Prior to cell seeding, culture flasks were coated with gelatin containing 0.02 mg/mL Fibronectin (F1141, Sigma Aldrich) and incubated at 37 °C for one hour. Subsequently, cells were passaged at a ratio of 1:4 upon reaching full confluence. The detachment of cells from flasks was facilitated by the addition of trypsin (0.25%)/EDTA (Gibco, Waltham, MA, USA) and incubation at 37 °C for 5 minutes, followed by termination of the digestion process through dilution with culture medium. After centrifugation at 500 ×g for 5 minutes, the HL-1 cells were reseeded in new coated 100 mm dishes and maintained at 37 °C in 5% CO₂. Cells within 10 passages post-thawing, procured from Sigma Aldrich (SCC065), were employed for subsequent experiments. To delineate the atrial myocardial characteristics of HL-1 cells, immunofluorescence staining utilizing atrial cardiomyocyte-specific marker protein Atrial Natriuretic Peptide (ANP) and cardiomyocyte marker cTnT was conducted, with the ventricular myocardial cell line H9c2 serving as a control. Ibrutinib powder, procured from MedChemExpress (MCE) (PCI-32765, MCE, Shanghai, China), was prepared in DMSO as a 100 µM stock. The range of ibrutinib concentrations (0, 0.01, 0.1, 1, 10, or 100 μM) was selected based on previous *in vitro* studies [21].

2.3 Western Blotting Analysis

We used western blotting (WB) to measure the expression levels of autophagy marker proteins, including Beclin-1 (1:2000, Abcam, Cambridge, UK, ab207612), Atg5 (1:1000, CST, Boston, MA, USA, 2630s), LC3B (1:500, Abmart Shanghai Co, Shanghai, China, T55992), and P62 (1:1000, CST, 88588s), as well as Cx43 (1:2000, Abcam, ab217676) and Cx40 (1:2000, Abcam, ab183648). The levels of phosphorylated-Bruton's tyrosine kinase (p-BTK) (1:2000, Abcam, ab68217), BTK (1:1000, CST, 8547s), mTOR (1:1000, CST, 2972s), p-mTOR (1:1000, CST, 5536s), PI3K (1:3000, CST, 4255s), p-PI3K (1:3000, CST, 4249s), Akt (1:2000, CST, 4685s) and p-Akt (1:2000, CST, 4060T) were also measured. In brief, HL-1 cells were cultured with varying concentrations of ibrutinib for 72 hours. Protein extraction from the cells was performed using radioimmunoprecipitation assay lysis buffer (RIPA), and quantification was conducted utilizing a BCA Protein Assay Kit (23225, Thermo Fisher, Waltham, MA, USA). Subsequently, 30 µg of protein from each experimental group was separated via SDS-polyacrylamide gel electrophoresis (SDS-PAGE), followed by transfer onto polyvinylidene difluoride membranes (Millipore, Boston, MA, USA). Membranes were then blocked with 5% bovine serum albumin at room temperature for two hours and sub-



sequently incubated with primary antibodies overnight at 4 °C. The following day, membranes were washed thrice with Tris-buffered saline with Tween 20 (TBST) for 5 minutes each and then incubated with secondary antibodies for 2 hours. Visualization of proteins was achieved using the FD bio-pico enhanced chemiluminescence kit HRP (FD8030, FD bio, Hangzhou, Zhejiang, China), and protein expression levels were quantified using ImageJ software (NIH, Bethesda, MD, USA).

2.4 ELISA

Following the plating of an equivalent number of HL-1 cells in a six-well plate, we adhered to the protocol outlined in the instruction manual of the Mouse Bruton's Tyrosine Kinase Activity Assay Kit (FY-EM12093-0, Wuhan, Hubei, China) to lyse the HL-1 cells treated with varying concentrations of ibrutinib and extract the resulting supernatant for BTK activity assessment. Subsequently, the absorbance value was determined at a wavelength of 450 nm, and a standard curve was generated to calculate the active concentration of mouse BTK in the sample based on the optical density (OD) values

2.5 Calcein and PI Staining

The effects of ibrutinib on HL-1 cell viability were assessed using the Calcein-AM/propidium iodide (PI) kit (Beyotime). Cells were treated with varying concentrations of ibrutinib (0, 0.01, 0.1, 1, 10, or 100 µM) for 72 hours. Subsequently, cells were subjected to three washes with phosphate-buffered saline (PBS) and then incubated with 1x washing buffer containing Calcein-AM and propidium iodide in the dark at 37 °C for 30 minutes. Following incubation, the cells were visualized using a fluorescence microscope (Carl Zeiss, Oberkochen, canton Batten-Würburg, Germany) under dark conditions. Red fluorescence indicated dead cells, whereas green fluorescence indicated viable cells. The percentage of positive cells was quantified using Image-Pro software (version 7.0.1, NIH, Bethesda, MD, USA).

2.6 Imaging Cell Morphology

To visualize cell morphology using a Zeiss Axio Observer microscope, live cells were stained with wheat germ agglutinin (1 mg/mL, Sigma Aldrich) diluted to a ratio of 1:40 in Hanks' balanced salt solution (HBSS) supplemented with 1% bovine serum albumin. The staining process lasted for 10 minutes.

2.7 Immunofluorescence Staining

HL-1 cells were cultured on gelatin-coated coverslips, washed twice with PBS, and fixed with methanol at room temperature for 20 minutes. Subsequently, the cells were washed with PBS for 5 minutes and incubated with a solution comprising PBS, 0.2% Triton X-100, and 10% goat serum for 1 hour at room temperature. HL-1 cells

were then subjected to primary antibody incubation against Cx43 (Abcam, ab217676), Cx40 (Abcam, ab183648), α-actin (Abcam, ab90421), ANP (Proteintech, Wuhan, Hubei, China, 27426-1-AP), and cTNT (Abcam, ab209813) at 4 °C within a humid chamber for 2 hours. The secondary antibodies employed were 555-conjugated goat anti-rabbit and 488-conjugated goat anti-mouse antibodies, each diluted to 1:500 in 10% goat serum. Nuclei were counterstained with DAPI, and post-staining, samples were rinsed twice with PBS before mounting with antifade mounting media. Finally, visualization of the stained cells was conducted using a fluorescence microscope (Carl Zeiss, Jena, Germany) under dark conditions.

2.8 Transmission Electron Microscopy (TEM)

HL-1 cells were initially fixed with 2.5% glutaraldehyde for a duration of 1.5 hours, followed by detachment using a cell scraper. The cells underwent centrifugation at 1500 rpm for 5 minutes and were then subjected to fixation in 1% aqueous uranyl acetate for a period of 1 hour. Post-fixation, the HL-1 cells were subjected to dehydration using a series of graded acetone solutions (ranging from 30% to 100%) subsequent to thorough washing with distilled water. Ultrathin sections were prepared, impregnated, and embedded onto copper grids utilizing an appropriate kit. Finally, the prepared samples were examined utilizing a transmission electron microscope (JEM-1400Flash, Shanghai J&R Instrument Technology Co., Shanghai, China).

2.9 Quantitative Real-Time Polymerase Chain Reaction (qRT-PCR)

Total RNA was extracted from HL-1 cells cultured with either ibrutinib or the control condition. A total of 500 ng of total RNA was reverse-transcribed into cDNA with the Hifair 1st Strand cDNA Synthesis Super Mix kit (11119ES60, Yeasen Biotechnology, Shanghai, China). cDNA was quantified with specific primers for Cx43 and Cx40 using the Hieff UNICON power qPCR SYBR Green Master Mix kit (Yeasen Biotechnology). β -Actin was used as the housekeeping gene for data normalization. The reactions were incubated in a 96-well plate at 95 °C for 10 minutes, followed by 40 cycles at 95 °C for 10 seconds, 60 °C for 20 seconds and 72 °C for 20 seconds. The entire reactions were analyzed using a 7500 Fast Real-Time PCR System (Applied Biosystems, Waltham, MA, USA). The sequences of the Cx43-, Cx40-, and β -actin-specific primers are provided in **Supplementary Table 1**.

2.10 Optical Mapping

The HL-1 cells were stained with freshly prepared FluoVolt TM membrane potential dye (F10488, Thermo Fisher, Waltham, MA, USA). The medium was removed, and the cells were washed with physiological buffer and then incubated with prepared dye loading buffer containing Component B $(100\times)$ and Component A $(1000\times)$ at



room temperature for 30 minutes. The cells were washed twice, and then Neuro Backdrop Background Suppressor solution was added to the cells at a dilution ratio of 1:10. A Dhyana 400BSI V2 camera (2 kHz sampling rate, 100 × 100 pixels, 100 μm/pixel, SciMedia, Shanghai, China) was used to capture the images. Subsequently, the acquired images were analyzed using ElectroMap, an open-source software. We used a 5×5 pixel Gaussian spatial filter on the raw signal and linear top-hat filtering to correct nonphysiological changes in baseline fluorescence. A standalone conduction velocity module within ElectroMap was applied for conduction velocity measurement and the midpoint of depolarization was used to produce the activation maps [22]. Three groups were set: control, 1 μM ibrutinib, 50 µM Gap 27 (HY-P0139, MCE), a gap junction inhibitor. Thus, ElectroMap grams of HL-1 cell monolayers were recorded to generate the activation maps and analyze arrhythmia incidence and conduction velocity.

2.11 Calcium Transient Analysis

HL-1 cells were seeded onto glass coverslips and subsequently washed with Hanks' balanced salt solution (HBSS) prior to loading with 3 µM Fluo-4 AM (Invitrogen F14201). Following loading, the HL-1 cells were incubated in darkness at room temperature for 60 minutes. Upon completion of the incubation period, Fluo-4-loaded HL-1 cells were washed with HBSS and subjected to imaging using a Dhyana 400BSI V2 camera coupled with an Olympus IX71 inverted microscope (IX71-RC, Olympus, Tokyo, Japan). Videos capturing spontaneous calcium transients were recorded. For statistical analysis, twenty-five cells from both the control and ibrutinib-treated groups were included. Fiji software (Plot Z-axis profile, NIH, Bethesda, MD, USA) was employed to measure the average pixel intensity (F) in randomly selected regions, serving as a reflection of calcium activity. Relative changes in fluorescence were determined utilizing the formula: (F-F0)/F0, where F0 represents the fluorescence intensity at time 0. Arrhythmia incidence and transient calcium flux amplitude were assessed using calcium graphs.

2.12 Bioinformatics Analysis

We downloaded the relevant transcriptome [16] and proteomics data [23] of the left atrial appendage tissues from mice treated with Ibrutinib in previous studies. Initially, we conducted a statistical analysis to identify differentially expressed proteins and genes in the Ibrutinib intervention group compared to the control group. Subsequently, we performed consensus Kyoto Encyclopedia of Genes and Genomes (KEGG) analysis on the respective KEGG enrichment results derived from the differentially expressed proteomes and transcriptomes. A Venn diagram was then generated using the ggVennDiagram R package (https://cran.r-project.org/web/packages/ggVennDiagram/index.html) to

illustrate the overlapping pathways. Furthermore, based on the consensus KEGG differential genes, Gene Ontology (GO) pathway enrichment analyses were carried out employing the clusterProfiler 4.6.2 package (https://bioconductor.org/packages/release/bioc/html/clusterProfiler.html), with an adjusted *p* value threshold of less than 0.05 utilized as the cut-off criterion.

2.13 Statistical Analysis

The characteristics of the patients enrolled in the study were delineated in terms of the median (interquartile range), mean ± Standard deviation (SD), or median for quantitative variables based on the statistical normality test. Comparative analyses of non-normally distributed qualitative and quantitative variables were conducted using the chi-square test and Kruskal-Wallis test with Dunn's posttests, employing SPSS (IBM Corp., Chicago, IL, USA) and Prism version 8.3.1 software (https://www.graphpad.c om/updates/prism-830-release-notes). Similarly, data adhering to a normal distribution underwent analysis using the Kolmogorov-Smirnoff test. Fisher's exact test was employed to assess differences between proportions, followed by multiple comparisons correction utilizing the Bonferroni method. Curve Expert 1.3 software (Hyams Development, https://www.curveexpert.net/) was utilized for drawing the standard curve of BTK enzyme activity and calculating enzyme activity units in different samples. A significance level of p < 0.05 was deemed statistically significant.

3. Results

3.1 Clinical Investigation of Ibrutinib-Related Atrial Fibrillation in 187 CLL Patients

To ascertain the incidence of ibrutinib-induced atrial fibrillation in clinical practice, a cohort comprising one hundred eighty-seven chronic lymphocytic leukemia (CLL) patients undergoing ibrutinib therapy was recruited for our study (registered under clinical trial number: ChiCTR2100046062). Prior to treatment initiation, baseline electrocardiograms were conducted for all 187 patients, revealing sinus rhythm in each case (Supplementary Fig. 1B). Additionally, transthoracic echocardiograms demonstrated normal myocardial systolic function without evidence of valvular disease. Throughout a median follow-up period of 12 months post-treatment, five patients developed new-onset atrial arrhythmia, as discerned from electrocardiograms (Supplementary Fig. 1C). Detailed characteristics of these five patients are presented in Supplementary Fig. 1A.

3.2 Impact of Ibrutinib Exposure on HL-1 Cells

We exposed HL-1 cells to increasing concentrations (0, 0.01, 0.1, 1, 10, and 100 μ M) of ibrutinib to investigate its impact on BTK activity and cell viability. Significant inhibition of BTK was observed with ibrutinib treatment at doses exceeding 0.01 μ M, as depicted in Fig. 1A. Fur-



thermore, the inhibition effects of ibrutinib on BTK were found to manifest in a dose-dependent manner. Specifically, treatment with 1 μM ibrutinib resulted in a reduction of BTK activity to 46.6% of the control group (Fig. 1C), mirroring the suppression observed at concentrations of 0.1 μM and 10 μM (Supplementary Fig. 2). To assess the potential cytotoxicity of various concentrations of ibrutinib on HL-1 cells, we quantified cell viability using calcein-AM/PI staining. Our findings indicate that treatment with 0.01 μM to 10 μM ibrutinib elicited negligible cardiotoxic effects on HL-1 cells. Only the 100 μM dose resulted in a reduction of HL-1 cell viability by 4.2% (Fig. 1B,D). Based on the outcomes of these experiments, we identified 1 μM as an appropriate concentration of ibrutinib, demonstrating efficacy without inducing cytotoxicity.

3.3 Ibrutinib Enhanced Susceptibility to Atrial Arrhythmia by Decreasing Conduction Velocity

Given the prevalence of atrial fibrillation (AF) as the foremost atrial rhythm disorder associated with ibrutinib, our investigation aimed to assess whether ibrutinib could exacerbate susceptibility to atrial arrhythmia. Immunofluorescence staining for the atrial cardiomyocyte marker protein ANP (Supplementary Fig. 3) was employed to confirm the atrial myocardial properties of HL-1 cells. Subsequently, optical mapping was utilized to evaluate the arrhythmogenic effects on transient Ca2+ fluxes and action potential conduction in HL-1 cells. Prior to staining, to mitigate the influence of cell plating and uncontrolled growth on intercellular connections, live cell staining was conducted to ensure the formation of homogeneous monolayers in both the ibrutinib and control groups (Supplementary Fig. **4B**). Analysis of transient calcium fluxes revealed comparable frequencies and amplitudes between the groups treated with or without ibrutinib (Supplementary Fig. 5A-C). Notably, HL-1 cells treated with 1 µM ibrutinib for 24 hours exhibited a higher proportion of "reentry-like" activation mapping diagrams compared to controls (Supplementary Fig. 4A and Supplementary videos). A total of 450 recordings were analyzed, revealing a markedly increased incidence of re-entries in HL-1 cells treated with 1 μM ibrutinib alongside 50 μM Gap27 (a gap junction inhibitor employed as a positive control), with occurrences of 89.33% and 64%, respectively, compared to the control group, which exhibited an occurrence rate of 11.33% (Fig. 2C). Additionally, conduction velocity was quantified, demonstrating significantly reduced conduction velocity in the intervention group compared to controls (Fig. 2A,B).

3.4 Ibrutinib Decreased Connexin 43 and Connexin 40 Expression

Optical mapping analysis revealed a pronounced reduction in conduction velocity and an elevated incidence of re-entry in the ibrutinib-treated group. Electrical con-

duction among atrial cardiomyocytes is intricately linked to gap junction proteins such as Connexin 43 and 40. Moreover, we conducted an integrated analysis of transcriptomic sequencing [16] and proteomics [23] data from previous studies involving intraperitoneal injection of ibrutinib (25-30 mg/kg) in C57BL/6J mice. This analysis revealed enrichment of numerous differentially expressed proteins and genes (Supplementary Fig. 6A) in pathways related to ECM-receptor interaction KEGG and extracellular matrix structural constituent GO, both of which encompass connexins (Supplementary Fig. 6B–D). This underscores the pivotal role of connexins in the aberrant electrical conduction between cardiomyocytes induced by ibrutinib. According to qRT-PCR, ibrutinib treatment did not induce significant changes in the transcription levels of Connexin 43 and connexin 40 (Fig. 3A). However, Western blot analysis demonstrated a significant reduction in the protein levels of both Connexin 43 and Connexin 40 following ibrutinib treatment compared to the control group (Fig. 3B, C). Furthermore, immunofluorescence analysis was employed to evaluate the localization and abundance of Cx40 and Cx43. Consistently, a notable decrease in the fluorescence intensity of Cx40 and Cx43 was observed in the ibrutinib-treated group, without evident translocation (Fig. 3D,E). Our experimental findings indicate that while ibrutinib does not impact the expression of Cx43 or Cx40 at the transcriptional level, it significantly diminishes the expression of the functional protein units. These results align with the outcomes of our KEGG and GO analyses, which highlighted enrichment of the autophagic pathway and phagosome pathway (Supplementary Fig. 6B-D), suggesting that post-transcriptionally, the protein levels of Cx43 and Cx40 may be attenuated through degradation processes.

3.5 Ibrutinib Decreased Connexin 43 Expression by Enhancing Autophagic Activity via the PI3K/Akt/mTOR Pathway

A prior investigation noted elevated levels of the autophagy protein microtubule associated protein 1 light chain 3 beta (LC3B) in tumor cells of certain advanced CLL patients following standard ibrutinib treatment [24]. Furthermore, studies have demonstrated that ibrutinib can inhibit the PI3K/Akt/mTOR signaling pathway, thereby inducing autophagic cell death and mitigating cerebral ischemia/reperfusion injury [25].

Herein, representative transmission electron microscopy (TEM) images of HL-1 cells exhibited characteristic autophagic bodies with bilayer membrane structures and single-membrane autolysosomes in the ibrutinibtreated group (Fig. 4A). To further quantify autophagic levels, mCherry-GFP-LC3 viral transfection was employed to label autophagosomes and autolysosomes, facilitating assessment of the strength of the autophagic flux (Fig. 4B). The mCherry-GFP-LC3 protein participates in autophagosome formation, emitting yellow fluorescence owing to



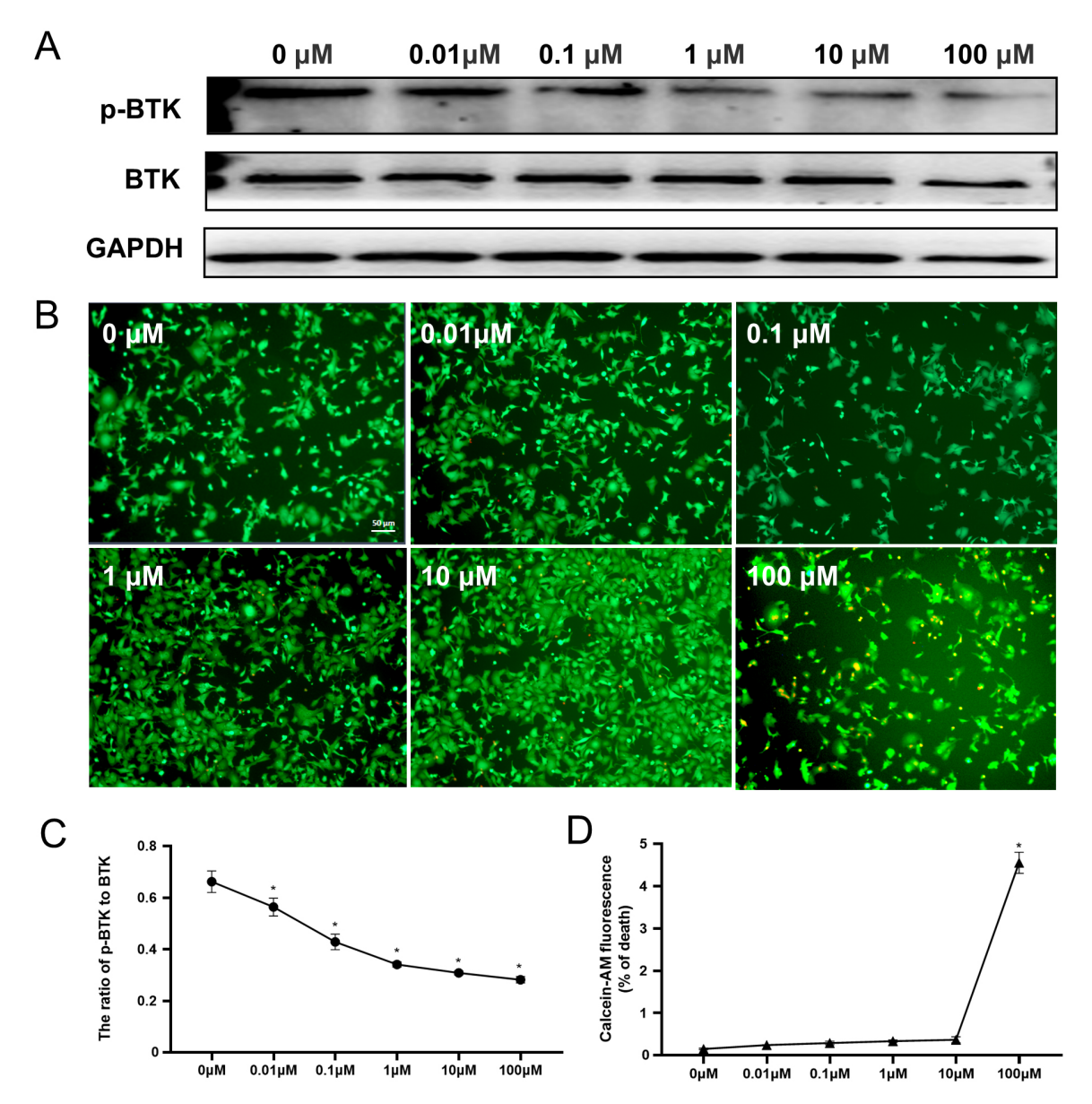


Fig. 1. Efficacy and toxicity of ibrutinib in HL-1 cells. (A,C) Western blotting of the P-BTK and BTK levels after treatment with different doses (0, 0.01, 0.1, 1, 10, or 100 μ M) of ibrutinib and statistical analysis. (B) Calcein and PI staining of cells treated with ibrutinib at various concentrations. Red fluorescence indicates dead cells, while green fluorescence indicates live cells. (D) Quantitative analysis of the dead cell ratio (red cells/green cells). All data are expressed as Mean \pm Standard deviation (SD) of three biological and three technical replicates for each treatment, *p < 0.05. HL-1, HL-1 Atrial Muscle Cell Line; BTK, Bruton's tyrosine kinase; p-BTK, phosphorylated Bruton's tyrosine kinase; GAPDH, Glyceraldehyde 3-phosphate dehydrogenase.

concurrent mCherry and GFP expression. Upon fusion of autophagosomes with lysosomes, the mCherry-GFP-LC3 protein emits solely red fluorescence due to GFP quenching in the acidic environment. Our findings revealed a significant increase in the numbers of intracellular green and red spots in the ibrutinib-treated group (Fig. 4C). Discrimination between autophagosomes and autophagolysosomes was achieved, with analysis indicating elevated vesicle counts following ibrutinib treatment (Fig. 4D).

Additionally, western blotting assays were employed to assess the expression of proteins involved in the upstream

autophagy-related PI3K/Akt/mTOR pathway, alongside autophagosome markers LC3I, LC3II, Beclin-1, and p62. Our results delineated the activation of autophagic flux from initiation to culmination stages in the ibrutinib-treated group. Exposure to ibrutinib suppressed PI3K/AKT/mTOR activity by inhibiting its phosphorylated expression, consequently activating autophagic flux. This activation was evidenced by the upregulation of ATG5 and Beclin-1, an elevated LC3II/LC3I ratio, and downregulation of p62 (Fig. 4E,F). Furthermore, hydroxychloroquine, an autophagy inhibitor, effectively counteracted the degradative



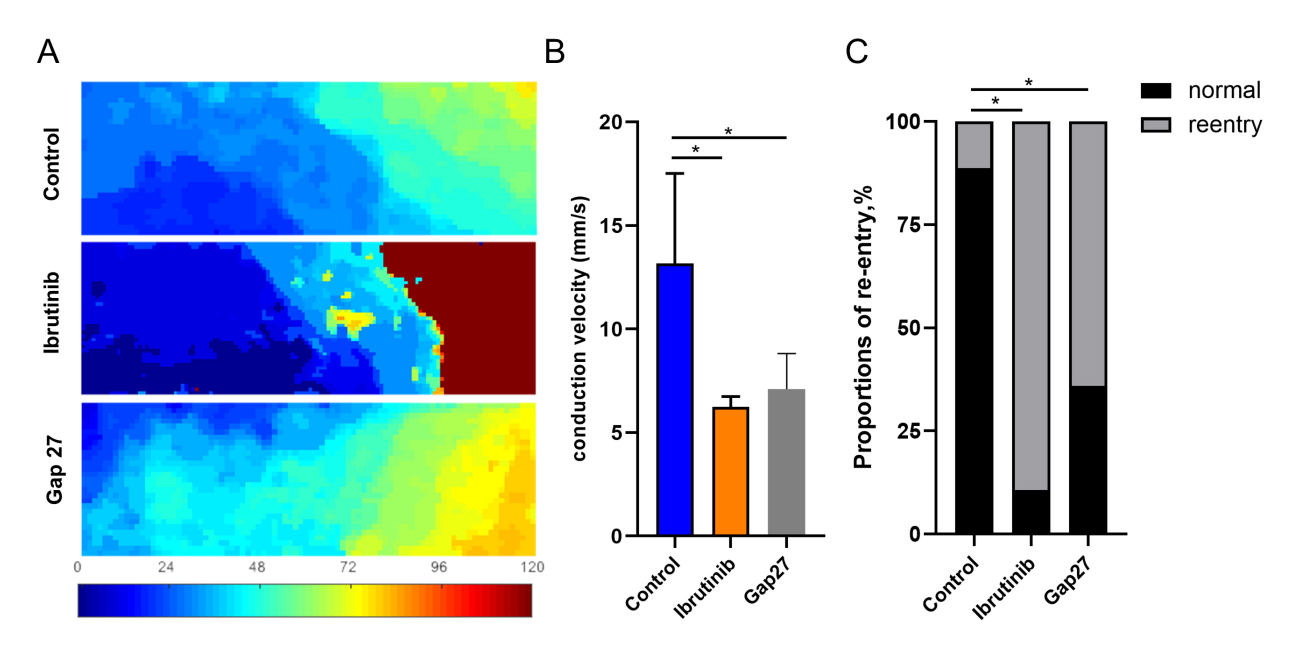


Fig. 2. Ibrutinib altered the conduction direction and velocity in cell monolayers. (A) Representative conduction velocity map of HL-1 cells monolayer with ibrutinib or Gap27 intervention. (B) Statistical analysis of the conduction velocity along the vector. n = 15 dishes for each group. (C) Statistical analysis of the proportion of re-entry or normal conduction events in the two groups, with an 89.33% re-entry occurrence rate in the ibrutinib group (n = 134/150), 64% in the Gap27 group (n = 96/150) and a 11.33% re-entry occurrence rate in the control group (n = 17/150), n = 150 videos of different fields of view captured on 15 dishes. *p < 0.05.

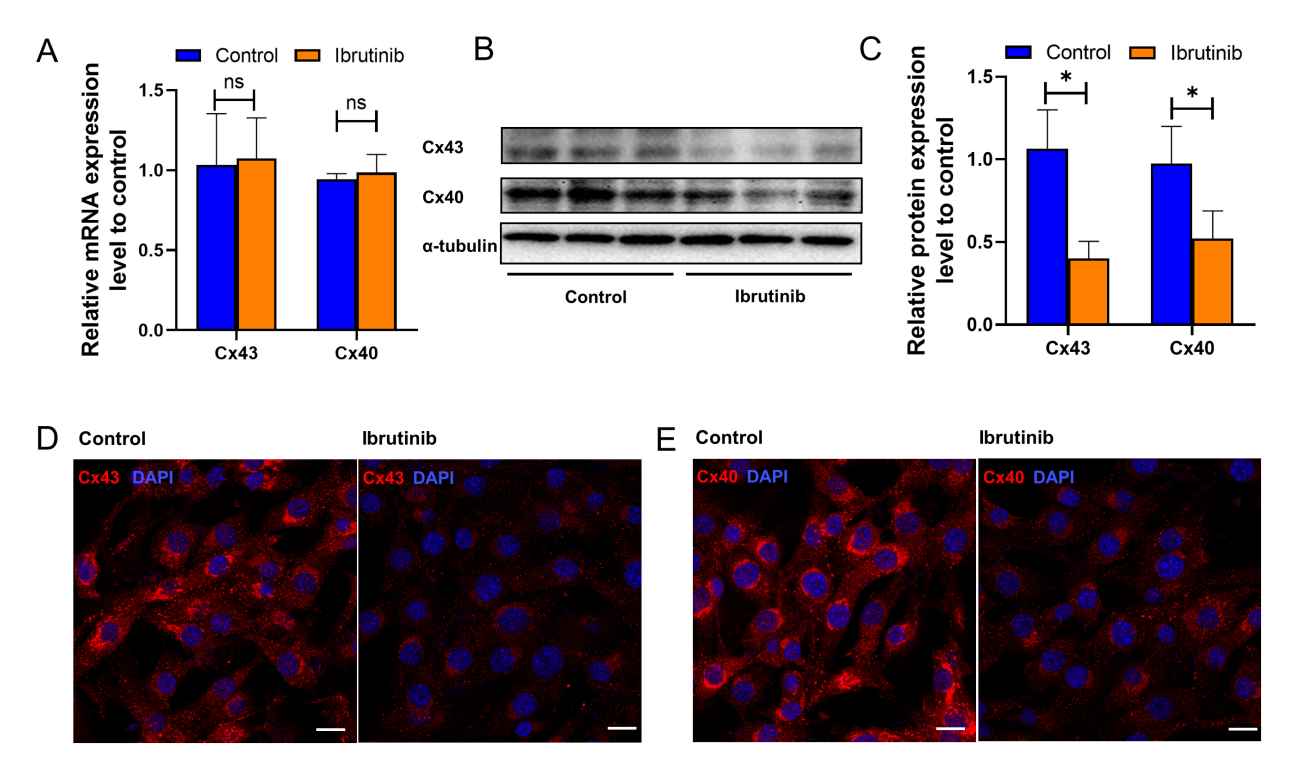


Fig. 3. Ibrutinib decreased Connexin43 and Connexin40 expression. (A) Quantitative real-time polymerase chain reaction (qRT-PCR) analysis of the gap junction proteins Gja1 (encodes Connexin43) and Gja5 (encodes Connexin40). The Messenger RNA (mRNA) levels of Gja1 and Gja5 were not statistically significantly different between the ibrutinib and control groups. (B) Representative Western blot of Connexin 40 and Connexin 43. α-Tubulin was used as the internal reference. (C) Statistical analysis of Connexin 40 and 43 protein expression in ibrutinib and control groups. (D, E) Representative immunofluorescence images of staining for 4′,6-diamidino-2-phenylindole (DAPI), Connexin43 and Connexin40 in HL-1 cells. The scale bar represents 50 μm. *p < 0.05; ns, non-significant.

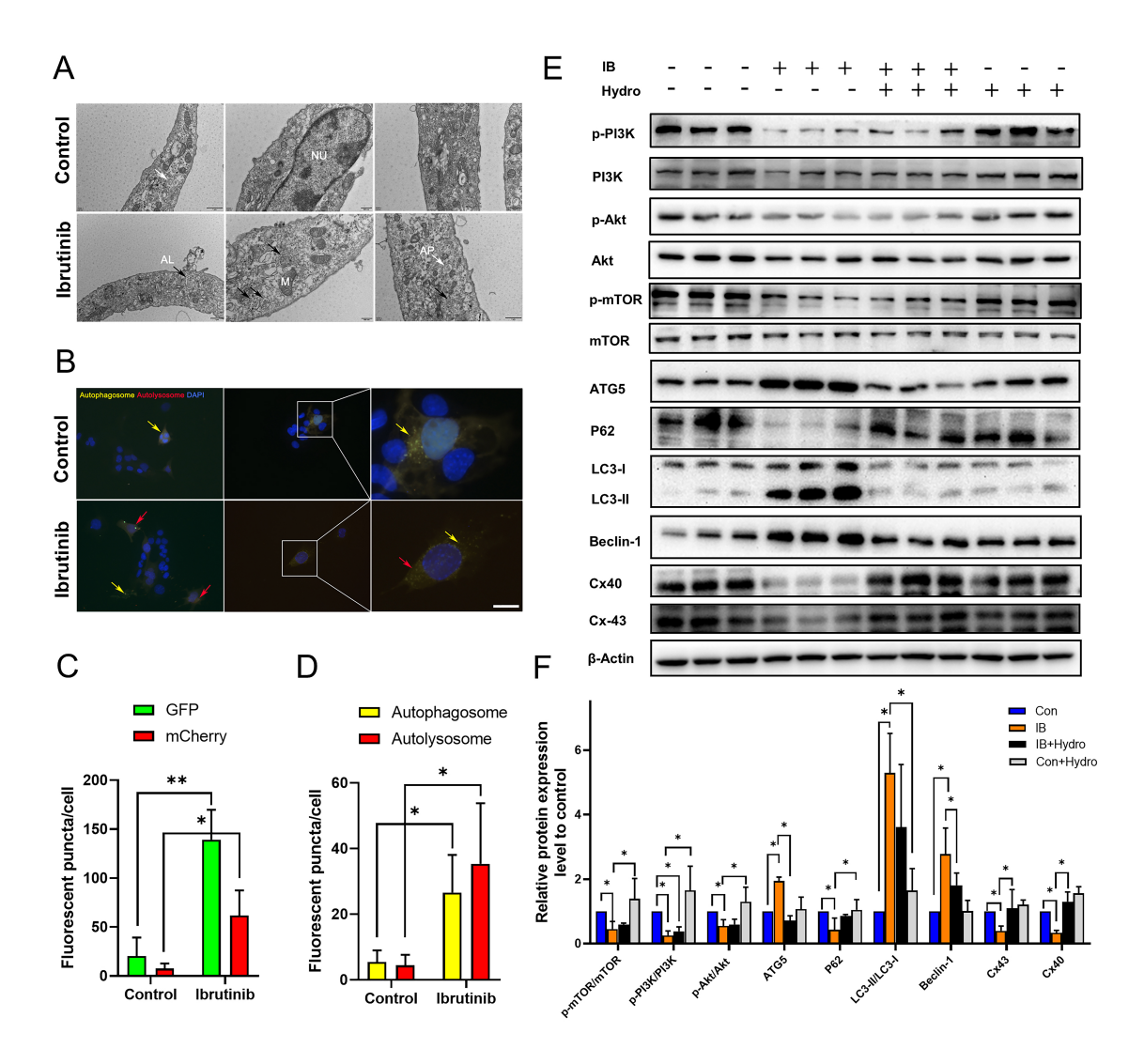


Fig. 4. Ibrutinib promotes Cx40 and Cx43 downregulation through autophagy. (A) Representative transmission electron microscope (TEM) images of HL1 cells treated with or without 1 μM ibrutinib. Nu, nucleus; Mt, mitochondrion; AP, autophagosome; AL, autolysosome. Bar shown on the bottom of the corresponding images. (B) Cells transfected with mCherry-GFP-LC3 virus for 24 hours before ibrutinib treatment for 24 hours were analyzed under a fluorescence microscope. Nuclei were stained with DAPI. Scale bar 50 μm. Yellow arrows, autophagosome and Red arrows, autolysosome. (C) Calculation of mCherry-GFP-LC3 puncta/cell with GFP puncta (green) and mCherry puncta (red), n = 50 cells for each group. (D) Analysis of mCherry-GFP-LC3 puncta/cell with yellow puncta (autophagosome) and red puncta (autolysosome), n = 50 cells for each group. (E) Representative Western blots of p-mTOR, mTOR, ATG5, LC3II/I, Beclin-1, P62, β-Actin, Beclin-1, p-PI3K, PI3K, p-Akt, Akt Cx43, and Cx40. (F) Statistical analysis of relative expression of proteins. IB, ibrutinib; Hydro, hydroxychloroquine; Con, control. *p < 0.05, *p < 0.01.

effects of ibrutinib on Cx43 and Cx40 proteins by reversing the autophagic process (Fig. 4E,F). Collectively, these findings suggest that ibrutinib augments the autophagic degradation of connexins through inhibition of the PI3K-AktmTOR pathway.

4. Discussion

4.1 Ibrutinib-Related Atrial Fibrillation is an Urgent Medical Problem

The high prevalence of atrial fibrillation associated with ibrutinib poses challenges to its clinical utility. Our

investigation revealed an incidence of atrial fibrillation at 2.7%, based on data collected at the Hematology Research Center of Jiangsu Province People's Hospital. Notably, this incidence rate slightly diverged from that reported in Jennifer R. Brown's clinical trial [26], which stood at 6.5%. Furthermore, ibrutinib administration correlates with a heightened risk of bleeding, thereby complicating the use of anticoagulants and presenting challenges in managing ibrutinib-induced atrial fibrillation [27]. Given the incomplete understanding of ibrutinib's proarrhythmic mechanisms, treatment decisions are hindered by a dearth of clin-



ical experience and experimental evidence. Hence, there is a pressing need for numerous studies to unravel the underlying mechanisms.

4.2 Slowing Conduction due to Abnormal Cell Connections Rather than Calcium Activity Plays a Key Role in the Development of Ibrutinib-Induced Atrial Fibrillation

Connexin proteins serve as principal mediators in facilitating the transmission of electric and metabolic signals among cardiomyocytes, thereby being indispensable for the maintenance of cardiac function. Various mutations identified in cardiac Cx40 and Cx43, including heterozygous missense mutations in GJA5 (G38D, P88S, A96S, and M163V) and GJA1 (c.932delC), have been associated with atrial fibrillation [28]. Notably, Leybaert et al. [29] reported that decreased connexin density at cellular poles, attributable to redistribution towards lateral margins, fosters conduction abnormalities, suggesting a potential substrate for atrial fibrillation within Cx43 remodeling. Given the pivotal role of both aberrant protein expression levels and lateralization of Cx43 and Cx40 in structurally predisposing arrhythmia [7], an evaluation of conduction associated with connexin proteins in ibrutinib-related atrial fibrillation is warranted. The HL-1 cell line, derived from atrial cardiomyocytes, was employed in our investigation to assess conduction at the cellular level. Acknowledging that the propagation of action potentials through gap junctions in a 2D homogeneous monolayer mirrors that in complex 3D models [30], the arrhythmogenic impact of ibrutinib was evaluated using optical mapping with a high spatiotemporal resolution, facilitating visualization of propagation trajectories. Intriguingly, our study observed a notable delay in conduction within HL-1 cell monolayers, accompanied by the emergence of reentrant-like waves. However, the differences in transient calcium fluxes between the control and intervention groups did not attain statistical significance. These findings suggest that the deceleration of conduction attributable to abnormal cell connections may constitute a pivotal factor in the pathogenesis of ibrutinib-induced atrial fibrillation.

4.3 Ibrutinib-Induced Connexin Degradation Occurs due to the Activation of Autophagy via Its Off-Target Effect on the PI3K-AKT-mTOR Signaling Pathway

Our research identified no disparity in the transcriptional expression of Cx43 and Cx40. However, notably diminished protein expression levels observed in the ibrutinib-treated group suggest a potential interference of the drug with post-transcriptional modification or degradation processes of connexin proteins. Autophagy, a crucial degradation mechanism in eukaryotes, plays a pivotal role in maintaining normal physiological functions. Various stressors, including hypoxia, nutrient deprivation, and cytotoxic agents, can induce autophagy [31]. Prior studies have demonstrated the ability of apelin-13 to counteract Ang II-induced Cx43 downregulation by mitigating in-

creased autophagy [32]. Connexins can undergo degradation via autophagy-mediated formation of autophagic lysosomes [33]. Lu et al. [34] observed myocardial ischemiareperfusion injury-induced Cx43 remodeling through autophagy. Our investigation revealed heightened degradation of Cx43 and Cx40 alongside augmented autophagic flux following ibrutinib treatment. Several reports have also highlighted ibrutinib's role as an inducer of autophagy in antitumor therapy, evidenced in conditions such as glioblastoma [35] and skin cancer [36]. Consequently, our endeavor aimed to elucidate the potential mechanistic linkages among ibrutinib, Cx43, autophagy, and atrial fibrillation. Ibrutinib, a well-established small-molecule inhibitor targeting Bruton's tyrosine kinase (BTK), exerts its effects by selectively and irreversibly binding to BTK, thereby inhibiting its enzymatic activity and disrupting pro-survival signals stemming from B cell receptor (BCR) inactivation. Notably, ibrutinib can impede downstream molecules within the BCR pathway, including PI3K, AKT, and Erk [37]. Of particular relevance, the PI3K/Akt/mTOR pathway serves as a critical regulator of autophagy [38]. Confirmation of the PI3K/Akt/mTOR pathway's activity in HL-1 cells treated with 1 µM ibrutinib was established in our present study.

4.4 Ibrutinib Combined with Autophagy Inhibitors might have Broad Clinical Applications in Treating CLL Patients

In our investigation, the autophagy inhibitor hydroxychloroquine demonstrated the capacity to mitigate the decline in Cx43 and Cx40 expression, thereby ameliorating aberrant conduction in HL-1 cell monolayers. Furthermore, ibrutinib exhibited inhibitory effects on skin cancer cell proliferation, a phenomenon notably potentiated in the presence of 3MA, an autophagy inhibitor [36]. Likewise, the augmentation of ibrutinib's anticancer activity in glioblastoma was observed upon autophagy inhibition by 3MA in vivo [35]. Moreover, the autophagy flux was inhibited in CLL cells via post-transcriptional modulation by chidamide, which could induce cytotoxicity [39]. Ibrutinib, as a pioneering therapeutic agent for CLL treatment, is widely prescribed and well-tolerated, manifesting rapid and enduring responses. Nonetheless, atrial fibrillation, a prevalent adverse effect, often necessitates therapy discontinuation in clinical trials [40]. The precise mechanism underlying ibrutinib's off-target cardiac effects remains incompletely elucidated. However, our findings offer a novel hypothesis: ibrutinib induces connexin degradation, thereby elevating the incidence of re-entry phenomena in vitro. Considering our study alongside prior investigations, the potential therapeutic synergy of ibrutinib in combination with autophagy inhibitors in CLL patients warrants consideration. Such a combination regimen may yield enhanced tumor cytotoxicity and a reduced occurrence of ibrutinib-induced atrial fibrillation.



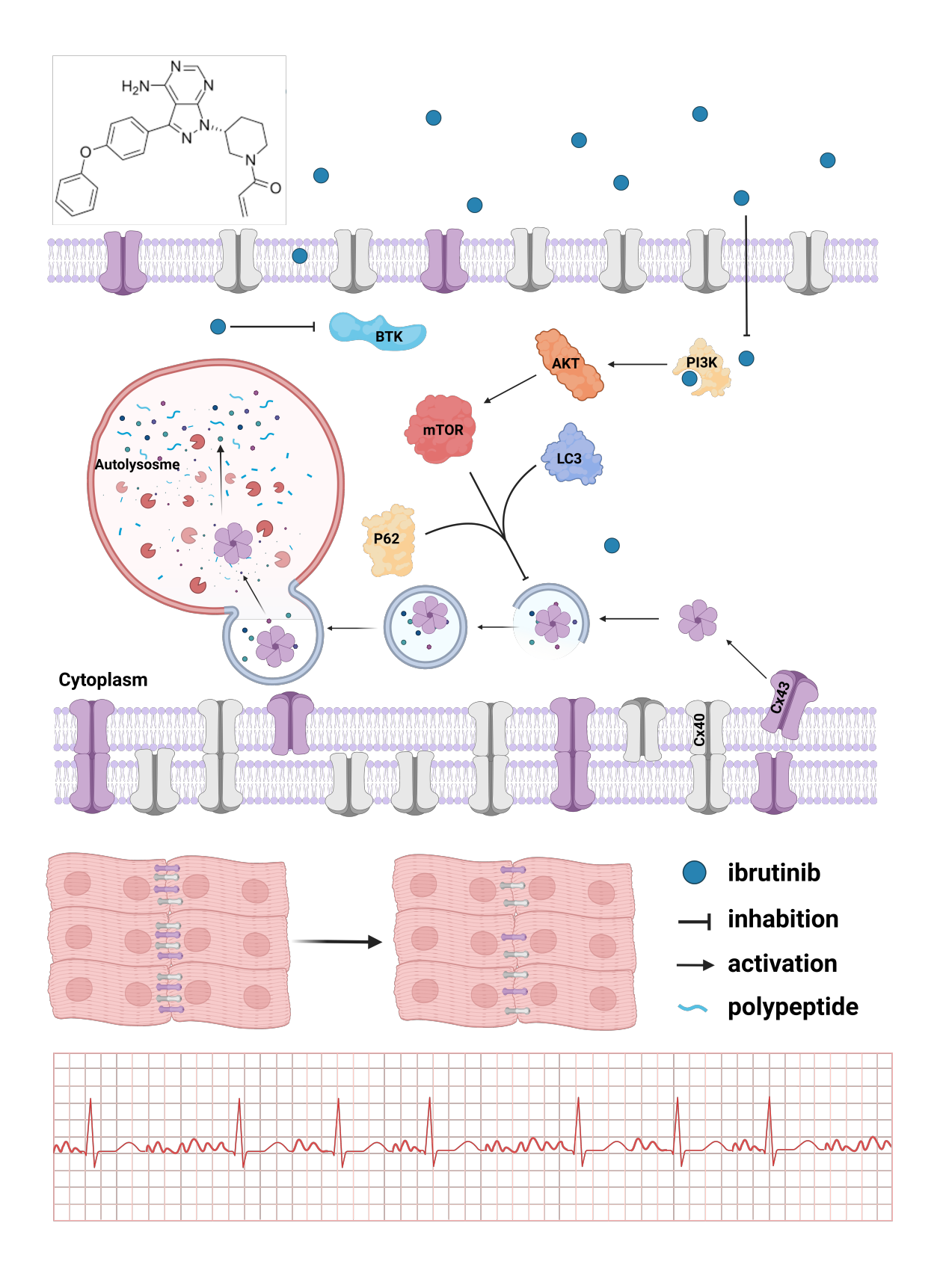


Fig. 5. Schematic diagram. Showing ibrutinib decreases Cx43 and Cx40 expression by inducing autophagy via the PI3K-AKT-mTOR signaling pathway in HL-1 cells. As a result, the decreased expression of Cx43 and Cx40 increases susceptibility to atrial fibrillation. (Created with https://www.biorender.com/).

5. Conclusions

In our current investigation, we have uncovered a notable finding regarding the potential of ibrutinib to heighten susceptibility to atrial fibrillation in patients with CLL. Subsequent research has elucidated an association between ibrutinib-induced conduction abnormalities and the down-regulation of Connexin 40 and 43. Moreover, heightened autophagic activity has been identified as a contributing factor to the decreased expression of Connexin 40 and 43. Notably, intervention through autophagy inhibition in HL-1 cells resulted in a substantial reversal of the degradation process. These findings suggest that targeting autophagy holds promise as a viable approach to mitigate ibrutinib-related atrial arrhythmia (Fig. 5).

Availability of Data and Materials

The study's supporting data are available on request from the corresponding author.

Author Contributions

ZW, CC, and MC designed the research. HQ and BZ performed the research. YJ, HZ and CW collected and analyzed the clinical data of CLL patients. HQ and ZL analyzed the experiment data and drew figures and supplementary figures. HQ and CW wrote the manuscript. All authors have participated sufficiently in the work to take public responsibility for appropriate portions of the content and agreed to be accountable for all aspects of the work in ensuring that questions related to its accuracy or integrity. All authors read and approved the final manuscript. All authors contributed to editorial changes in the manuscript.

Ethics Approval and Consent to Participate

The clinical study was established, according to the ethical guidelines of the Helsinki Declaration and was approved by the Human Ethics Committee of The First Affiliated Hospital of Nanjing Medical University (2021-SR-006). Written informed consent was obtained from individual or guardian participants.

Acknowledgment

We would like to thank Dongxia Ji, Meng Sun, and Sanli Li (Feiyuebio, Wuhan, China) for working overtime during the Chinese Spring Festival to provide us with the ELISA kit.

Funding

This work was supported by a grant from the National Nature Science Foundation of China [grant number: 82100338 to Cheng Wang].

Conflict of Interest

The authors declare no conflict of interest.

Supplementary Material

Supplementary material associated with this article can be found, in the online version, at https://doi.org/10.31083/j.fbl2905201.

References

- [1] Thompson PA, Lévy V, Tam CS, Al Nawakil C, Goudot FX, Quinquenel A, *et al*. Atrial fibrillation in CLL patients treated with ibrutinib. An international retrospective study. British Journal of Haematology. 2016; 175: 462–466.
- [2] Salem JE, Manouchehri A, Bretagne M, Lebrun-Vignes B, Groarke JD, Johnson DB, *et al.* Cardiovascular Toxicities Associated With Ibrutinib. Journal of the American College of Cardiology. 2019; 74: 1667–1678.
- [3] Farooqui M, Valdez J, Soto S, Bray A, Tian X, Wiestner A. Atrial Fibrillation in CLL/SLL Patients on Ibrutinib. Blood. 2015; 126: 2933–2933.
- [4] Wang K, Zhao J, Guo Z. Interaction of KCNA5, CX43, and CX40 proteins in the atrial muscle of patients with atrial fibrillation. Cell Biology International. 2022; 46: 1834–1840.
- [5] Yeager M. Structure of cardiac gap junction intercellular channels. Journal of Structural Biology. 1998; 121: 231–245.
- [6] Paul M, Wichter T, Gerss J, Arps V, Schulze-Bahr E, Robenek H, et al. Connexin expression patterns in arrhythmogenic right ventricular cardiomyopathy. The American Journal of Cardiology. 2013; 111: 1488–1495.
- [7] Dhein S, Salameh A. Remodeling of Cardiac Gap Junctional Cell-Cell Coupling. Cells. 2021; 10: 2422.
- [8] Lin X, Gemel J, Glass A, Zemlin CW, Beyer EC, Veenstra RD. Connexin40 and connexin43 determine gating properties of atrial gap junction channels. Journal of Molecular and Cellular Cardiology. 2010; 48: 238–245.
- [9] Hegner P, Lebek S, Tafelmeier M, Camboni D, Schopka S, Schmid C, et al. Sleep-disordered breathing is independently associated with reduced atrial connexin 43 expression. Heart Rhythm. 2021; 18: 2187–2194.
- [10] Magyar J, Banyasz T, Szentandrassy N, Kistamas K, Nanasi PP, Satin J. Role of gap junction channel in the development of beatto-beat action potential repolarization variability and arrhythmias. Current Pharmaceutical Design. 2015; 21: 1042–1052.
- [11] Levine B, Klionsky DJ. Development by self-digestion: molecular mechanisms and biological functions of autophagy. Developmental Cell. 2004; 6: 463–477.
- [12] Martins-Marques T, Catarino S, Marques C, Pereira P, Girão H. To beat or not to beat: degradation of Cx43 imposes the heart rhythm. Biochemical Society Transactions. 2015; 43: 476–481.
- [13] Martins-Marques T, Ribeiro-Rodrigues T, Batista-Almeida D, Aasen T, Kwak BR, Girao H. Biological Functions of Connexin43 Beyond Intercellular Communication. Trends in Cell Biology. 2019; 29: 835–847.
- [14] Bejarano E, Yuste A, Patel B, Stout RF, Jr, Spray DC, Cuervo AM. Connexins modulate autophagosome biogenesis. Nature Cell Biology. 2014; 16: 401–414.
- [15] Sestier M, Hillis C, Fraser G, Leong D. Bruton's tyrosine kinase Inhibitors and Cardiotoxicity: More Than Just Atrial Fibrillation. Current Oncology Reports. 2021; 23: 113.
- [16] Xiao L, Salem JE, Clauss S, Hanley A, Bapat A, Hulsmans M, et al. Ibrutinib-Mediated Atrial Fibrillation Attributable to Inhibition of C-Terminal Src Kinase. Circulation. 2020; 142: 2443– 2455.
- [17] Tang H, Li J, Liu X, Wang G, Luo M, Deng H. Down-regulation of HSP60 Suppresses the Proliferation of Glioblastoma Cells via the ROS/AMPK/mTOR Pathway. Scientific Reports. 2016; 6: 28388.



- [18] Dong R, Yan Y, Zeng X, Lin N, Tan B. Ibrutinib-Associated Cardiotoxicity: From the Pharmaceutical to the Clinical. Drug Design, Development and Therapy. 2022; 16: 3225–3239.
- [19] Hallek M, Cheson BD, Catovsky D, Caligaris-Cappio F, Dighiero G, Döhner H, et al. Guidelines for the diagnosis and treatment of chronic lymphocytic leukemia: a report from the International Workshop on Chronic Lymphocytic Leukemia updating the National Cancer Institute-Working Group 1996 guidelines. Blood. 2008; 111: 5446–5456.
- [20] Claycomb WC, Lanson NA, Jr, Stallworth BS, Egeland DB, Delcarpio JB, Bahinski A, et al. HL-1 cells: a cardiac muscle cell line that contracts and retains phenotypic characteristics of the adult cardiomyocyte. Proceedings of the National Academy of Sciences of the United States of America. 1998; 95: 2979– 2984.
- [21] Tuomi JM, Bohne LJ, Dorey TW, Jansen HJ, Liu Y, Jones DL, et al. Distinct Effects of Ibrutinib and Acalabrutinib on Mouse Atrial and Sinoatrial Node Electrophysiology and Arrhythmogenesis. Journal of the American Heart Association. 2021; 10: e022369.
- [22] O'Shea C, Holmes AP, Yu TY, Winter J, Wells SP, Correia J, et al. ElectroMap: High-throughput open-source software for analysis and mapping of cardiac electrophysiology. Scientific Reports. 2019; 9: 1389.
- [23] Yang X, An N, Zhong C, Guan M, Jiang Y, Li X, et al. Enhanced cardiomyocyte reactive oxygen species signaling promotes ibrutinib-induced atrial fibrillation. Redox Biology. 2020; 30: 101432.
- [24] Arroyo DS, Rodriguez CM, Bussi C, Manzone-Rodriguez C, Sastre D, Heller V, et al. Increased Expression of Autophagy Protein LC3 in Two Patients With Progressing Chronic Lymphocytic Leukemia. Frontiers in Endocrinology. 2020; 11: 321.
- [25] Jin L, Mo Y, Yue EL, Liu Y, Liu KY. Ibrutinib ameliorates cerebral ischemia/reperfusion injury through autophagy activation and PI3K/Akt/mTOR signaling pathway in diabetic mice. Bioengineered. 2021; 12: 7432–7445.
- [26] Brown JR, Moslehi J, O'Brien S, Ghia P, Hillmen P, Cymbalista F, et al. Characterization of atrial fibrillation adverse events reported in ibrutinib randomized controlled registration trials. Haematologica. 2017; 102: 1796–1805.
- [27] Kapelios CJ, Bonou MS, Diamantopoulos P, Angelopoulou MK, Masoura C, Barbetseas J, et al. Ibrutinib-related atrial fibrillation: Therapeutic challenges. Journal of Oncology Pharmacy Practice: Official Publication of the International Society of Oncology Pharmacy Practitioners. 2019; 25: 1258–1260.
- [28] Thibodeau IL, Xu J, Li Q, Liu G, Lam K, Veinot JP, et al.

- Paradigm of genetic mosaicism and lone atrial fibrillation: physiological characterization of a connexin 43-deletion mutant identified from atrial tissue. Circulation. 2010; 122: 236–244.
- [29] Leybaert L, Lampe PD, Dhein S, Kwak BR, Ferdinandy P, Beyer EC, et al. Connexins in Cardiovascular and Neurovascular Health and Disease: Pharmacological Implications. Pharmacological Reviews. 2017; 69: 396–478.
- [30] Houston C, Tzortzis KN, Roney C, Saglietto A, Pitcher DS, Cantwell CD, et al. Characterisation of re-entrant circuit (or rotational activity) in vitro using the HL1-6 myocyte cell line. Journal of Molecular and Cellular Cardiology. 2018; 119: 155–164.
- [31] Huang J, Klionsky DJ. Autophagy and human disease. Cell Cycle (Georgetown, Tex.). 2007; 6: 1837–1849.
- [32] Chen Y, Qiao X, Zhang L, Li X, Liu Q. Apelin-13 regulates angiotensin ii-induced Cx43 downregulation and autophagy via the AMPK/mTOR signaling pathway in HL-1 cells. Physiological Research. 2020; 69: 813–822.
- [33] Fong JT, Kells RM, Gumpert AM, Marzillier JY, Davidson MW, Falk MM. Internalized gap junctions are degraded by autophagy. Autophagy. 2012; 8: 794–811.
- [34] Lu Q, Li W, Li Z, Chen Z, Fu W, Jiang Q, *et al*. Effect of autophagy on cardiomyocyte membrane Cx43 acute remodeling in rats with ischemia-reperfusion. International Journal of Clinical and Experimental Pathology. 2019; 12: 2639–2645.
- [35] Wang J, Liu X, Hong Y, Wang S, Chen P, Gu A, *et al.* Ibrutinib, a Bruton's tyrosine kinase inhibitor, exhibits antitumoral activity and induces autophagy in glioblastoma. Journal of Experimental & Clinical Cancer Research: CR. 2017; 36: 96.
- [36] Sun FD, Wang PC, Shang J, Zou SH, Du X. Ibrutinib presents antitumor activity in skin cancer and induces autophagy. European Review for Medical and Pharmacological Sciences. 2018; 22: 561–566.
- [37] Ondrisova L, Mraz M. Genetic and Non-Genetic Mechanisms of Resistance to BCR Signaling Inhibitors in B Cell Malignancies. Frontiers in Oncology. 2020; 10: 591577.
- [38] Al-Bari MAA, Xu P. Molecular regulation of autophagy machinery by mTOR-dependent and -independent pathways. Annals of the New York Academy of Sciences. 2020; 1467: 3–20.
- [39] Kong YL, Pan BH, Liang JH, Zhu HY, Wang L, Xia Y, et al. Chidamide, a histone deacetylase inhibitor, inhibits autophagy and exhibits therapeutic implication in chronic lymphocytic leukemia. Aging. 2020; 12: 16083–16098.
- [40] Estupiñán HY, Berglöf A, Zain R, Smith CIE. Comparative Analysis of BTK Inhibitors and Mechanisms Underlying Adverse Effects. Frontiers in Cell and Developmental Biology. 2021; 9: 630942.

